

## Co-acquisition of mineral-bound iron and phosphorus by natural *Trichodesmium* colonies

Yeala Shaked <sup>1,2\*</sup>, Dirk de Beer,<sup>3</sup> Siyuan Wang <sup>1,2</sup>, Futing Zhang <sup>1,2</sup>, Anna-Neva Visser <sup>1,2</sup>,  
Meri Eichner <sup>4</sup>, Subhajt Basu <sup>1,2,3,5</sup>

<sup>1</sup>The Freddy and Nadine Herrmann Institute of Earth Sciences, Edmond J. Safra Campus, Givat Ram, Hebrew University of Jerusalem, Jerusalem, Israel

<sup>2</sup>The Interuniversity Institute for Marine Sciences in Eilat, Eilat, Israel

<sup>3</sup>Max Planck Institute for Marine Microbiology (MPI Bremen), Bremen, Germany

<sup>4</sup>Laboratory of Photosynthesis, Center Algatech, Institute of Microbiology of the Czech Academy of Sciences, Třeboň, Czech Republic

<sup>5</sup>University of Petroleum and Energy Studies (UPES-SoHST), Dehradun, India

### Abstract

Low iron (Fe) and phosphorus (P) ocean regions are often home to the globally important N<sub>2</sub>-fixing cyanobacterium *Trichodesmium* spp., which are physiologically adapted to Fe/P co-limitation. Given *Trichodesmium*'s eminent ability to capture particles and the common associations between Fe and P in sediments and aerosols, we hypothesized that mineral bio-dissolution by *Trichodesmium* spp. may enable them to co-acquire Fe and P. We present a new sensitive assay to determine P uptake from particles, utilizing <sup>33</sup>P-labeled ferrihydrite. To validate the method, we examined single natural *Trichodesmium thiebautii* colonies in a high-resolution radio-tracer β-imager, identifying strong colony-mineral interactions, efficient removal of external <sup>33</sup>P-labeled ferrihydrite, and elevated <sup>33</sup>P uptake in the colony core. Next, we determined bulk P uptake rates, comparing natural Red Sea colonies and P-limited *Trichodesmium erythraeum* cultures. Uptake rates by natural and cultured *Trichodesmium* were similar to P release rates from the mineral, suggesting tight coupling between dissolution and uptake. Finally, synthesizing P-ferrihydrite labeled with either <sup>33</sup>P or <sup>55</sup>Fe, we probed for Fe/P co-extraction by common microbial mineral solubilization pathways. Dissolution rates of ferrihydrite were accelerated by exogenous superoxide and strong Fe-chelator and subsequently enhanced <sup>33</sup>P release and uptake by *Trichodesmium*. Our method and findings can facilitate further Fe/P co-acquisition studies and highlight the importance of biological mechanisms and microenvironments in controlling bioavailability and nutrient fluxes from particles.

Iron (Fe) and Phosphorus (P) play a central biogeochemical role in marine and freshwater environments by supporting primary productivity, carbon fixation, and drawdown from the atmosphere (Elser et al. 2007; Tagliabue et al. 2017;

Duhamel et al. 2021). Phytoplankton, the base of all aquatic food chains, require Fe and P for growth but can internalize these nutrients only as soluble inorganic and organic molecules (Shaked et al. 2005; Dyhrman 2016). The combination of high biological demand and low supply of dissolved nutrients to stratified and illuminated surface waters often renders Fe and P as limiting nutrients for phytoplankton growth in lakes, estuaries, and vast ocean regions (Moore et al. 2013; Browning et al. 2022).

Particulate nutrients are transported to the ocean via the atmosphere or rivers and are further distributed in the water column through sediment resuspension. Typically, researchers addressing particle-bound nutrients refer to organic matter bound to marine aggregates, which, in turn, are considered to act as a primary vehicle for nutrient transportation from the ocean surface to depth (Grossart et al. 2003; Decho and Gutierrez 2017). Despite significant particle loss near the

\*Correspondence: yeala.shaked@mail.huji.ac.il

This is an open access article under the terms of the [Creative Commons Attribution](https://creativecommons.org/licenses/by/4.0/) License, which permits use, distribution and reproduction in any medium, provided the original work is properly cited.

Additional Supporting Information may be found in the online version of this article.

**Author Contribution Statement:** Y.S., S.B., D.B., and M.E. conceptualized and designed the study. S.B. conducted the experiments with contribution from A.N., S.W., and F.Z. The data analysis was performed by Y.S., S.B., D.B., and A.N. Y.S. wrote the manuscript, and S.W. designed the graphs. All authors contributed to the writing or revision of the manuscript.

continents and to deep water, plumes of colloidal and particulate minerals were found to persist over long distances from the shore and disperse far away from hydrothermal sources (Lam and Bishop 2008; Boyd et al. 2010; Fitzsimmons et al. 2017). Similarly, some of the aerosols deposited on the ocean surface may remain in the euphotic zone for relatively long periods, and thus potentially serve as a significant nutrient source (Boyd et al. 2010; Leeuw et al. 2014; Ellwood et al. 2018). Yet, the bioavailability of these particles to phytoplankton requiring dissolved nutrients is often limited, since Fe and P minerals are poorly soluble in oxygenated and semi-neutral pH surface water (Baker et al. 2006; Journet et al. 2008; Anderson et al. 2010).

The biogeochemical cycles of Fe and P are linked, since iron(III)oxyhydroxides, which are ubiquitous in near-surface soils and sediments, interact strongly with dissolved phosphate via sorption, co-precipitation, mineral transformation, and redox-cycling reactions (Jaisi et al. 2010; McConnell et al. 2020). The mineralogical associations between Fe and P are complex, including iron(III) oxyhydroxide-phosphate (i.e., structurally bound P) as well as P fractions which are adsorbed and/or precipitated on the iron(III)oxyhydroxide surfaces (Li et al. 2016; McConnell et al. 2020). In soils and sediments, the operationally defined P-bound Fe fraction typically accounts for 10–30% of the particulate P pool (Aydin et al. 2009). Striving to obtain these valuable nutrients, plants, and their associated microbiomes employ diverse mechanisms for dissolving these minerals including local acidification, metabolite secretion, and electron transfer (Alori et al. 2017; Uroz et al. 2022). These pathways differ in their specificity, but in conjunction increase the flux of multiple dissolved nutrients and elements (including toxic metals). Since P is often associated with Fe minerals, pathways involving reductive or ligand-promoted dissolution are expected to increase both Fe and P supply to microorganisms and plants (Romano et al. 2017; McRose and Newman 2021; Cui et al. 2022).

In aquatic systems, organic aggregates, as well as phytoplankton colonies, decaying blooms, fecal pellets, gels, biofilms, and marine snow are considered hot spots of microbial activity that can harbor chemically distinct microenvironments (Simon et al. 2002; Grossart et al. 2003). These conditions may enhance the chemical and biological dissolution of minerals, likely increasing Fe and P bioavailability. Focusing on phytoplankton, colonies of globally important  $N_2$ -fixing cyanobacteria, *Trichodesmium* spp. might similarly enhance mineral dissolution since they are also considered as hot spots for phytoplankton–bacteria–mineral interactions (Frischkorn et al. 2017; Held et al. 2021; Qiu et al. 2022). Single *Trichodesmium* filaments often come together and form relatively large (~ 1 mm diameter) tuft-shaped and puff-shaped colonies. Research from our group and others demonstrated that natural colonies of *Trichodesmium* spp. hold unique capabilities to capture and actively transport dust to the colony core (Rueter et al. 1992; Rubin et al. 2011; Langlois et al. 2012;

Eichner et al. 2020). Following particle translocation to the colony's center, *Trichodesmium* and its associated bacteria were found to accelerate Fe-dissolution and thus increase Fe availability (Basu and Shaked 2018; Basu et al. 2019; Kessler et al. 2020b). As P and Fe minerals are associated, the pathways employed by the colony consortium to dissolve Fe minerals may also enhance P solubility and thus its bioavailability.

The prevalence of Fe–P minerals in natural environments clearly influences their importance in supplying P to *Trichodesmium* (and other phytoplankton). The most common P mineral in nature is apatite, a highly insoluble calcium phosphate-based mineral that contains no Fe (McConnell et al. 2020). Next in abundance in fluvial and shallow sediments are P-bound Fe minerals, including P minerals such as vivianite and amorphous  $Fe(PO_4)$  and P associated with iron oxyhydroxides (Gunnars et al. 2002; Egger et al. 2015; Duhamel et al. 2021). In reduced sediments and soils, mobilization of Fe and P during microbial respiration often result in formation of authigenic P-rich iron oxyhydroxides, where P may appear as impurities within minerals and/or precipitate or be adsorbed on the mineral surface (Borch et al. 2007; Jaisi et al. 2010; Ruttenger and Sulak 2011). In atmospheric aerosols, the fraction of P-bound Fe minerals varies according to the aerosol origin, mineralogy, size, and atmospheric processing (e.g., acidification, mixing with pollutants; Journet et al. 2008; Marcotte et al. 2020; Baker et al. 2021). The fraction of P-bound Fe minerals are relatively high in aerosols from biomass burning, fossil fuel combustion, and volcanic eruptions (Anderson et al. 2010; Tipping et al. 2014; Weinberger et al. 2016), but relatively low in Saharan dust (Baker et al. 2006; Nenes et al. 2011). Nonetheless, long-term transport of the apatite-rich Saharan dust over the Atlantic Ocean was shown to substantially increase the fraction of P-bound Fe (> 50%) as a result of atmospheric processing (Dam et al. 2021). These involve sharp changes in the pH of cloud droplets, shifting between acidic conditions that favors P release due to apatite dissolution and basic conditions that favor precipitation of Fe minerals that incorporate P (Shi et al. 2019).

Here, we quantify phytoplankton nutrient uptake from environmentally relevant  $^{33}P$ -labeled ferrihydrite, applying both bulk scintillation counting and high-resolution radio-tracer  $\beta$ -imaging. The choice of synthesizing Fe–P minerals labeled with  $^{33}P$  (or  $^{55}Fe$ ) entails several analytical benefits for the uptake assays and assists in exploring links between Fe and P bioavailability. Experimenting with natural Red Sea *Trichodesmium* colonies and P-limited cultures, we determined rates of P and Fe dissolution and uptake from particles. We further tested the role of reactive oxygen species and microbially produced iron-chelating agents in mineral dissolution and subsequent enhancement of Fe and P uptake. Our study demonstrates the high potential of this method to shed light on mechanistic details of particulate nutrient uptake.

## Materials and methods

### Overview

Studying solid-phase nutrient availability to phytoplankton entails a range of analytical challenges for obtaining reliable and reproducible uptake rates and maintaining an environmental context, such as low particle load and cell-particle proximity. Basu and Shaked (2018) resolved these challenges by optimizing a  $^{55}\text{Fe}$ -based method for investigating ferrihydrite availability to natural *Trichodesmium* colonies. Here, by synthesizing  $^{33}\text{P}$ -labeled ferrihydrite, we adjusted their method for studying availability of P-bound Fe minerals, which are highly abundant in soils, sediments and aerosols. See also supplementary information table S1 for further details on the challenges and achievements of the method.

### Fe-P particles: Synthesis and P release kinetics

#### Mineral synthesis

Most experiments were conducted between 2018 and 2019 and involved synthesis of two types of highly amorphous  $^{33}\text{P}$ -ferrihydrite minerals:  $^{33}\text{P}$ -adsorbed onto ferrihydrite and co-precipitated Fe- $^{33}\text{P}$ . The radioisotope  $^{33}\text{P}$  orthophosphoric acid purchased from Hartmann Analytic, Germany, has high activity but low P concentrations (specific activity  $3000\text{ Ci mmolP}^{-1}$ ). Hence, prior to synthesis, the  $^{33}\text{P}$  stock was diluted by unlabeled orthophosphoric acid, generating a lower specific activity working stock ( $50\text{ Ci mmolP}^{-1}$  or  $0.05\text{ }\mu\text{Ci }\mu\text{L}^{-1}$ ).  $^{33}\text{P}$ -adsorbed ferrihydrite was prepared by adding  $10\text{ nM P}$  from the working stock to  $500\text{ nM}$  amorphous ferrihydrite and allowed to react at pH 8.1 and  $25^\circ\text{C}$  for 24 h. Ferrihydrite was synthesized by titrating  $\text{FeCl}_3$  with  $0.1\text{ N NaOH}$  to pH 8.1 as earlier described (Basu and Shaked 2018). The  $^{33}\text{P}$ -adsorbed ferrihydrite was transferred to filtered seawater (FSW) and allowed to equilibrate for  $\sim 10\text{ d}$  to decrease the loosely bound P. Co-precipitated  $^{33}\text{P}$ -ferrihydrite mineral was synthesized by mixing  $1\text{ mM}$

$\text{FeCl}_3$  (pH 2) with  $0.7\text{ }\mu\text{M P}$  from the working stock and gradually increasing the solution pH to 8.1, via slow titration with  $0.1\text{ N NaOH}$ . Following synthesis, minerals were left to equilibrate in FSW for  $\sim 10\text{ d}$ .

In spring 2022,  $^{33}\text{P}$ -labeled ferrihydrite was synthesized again for studying the effect of superoxide on P dissolution and uptake. Minerals with varying P release rates were generated using different protocols as detailed in Supporting Information Note 1 and Table S2. In addition to the  $^{33}\text{P}$ -labeled minerals,  $^{55}\text{Fe}$ -labeled minerals were prepared using same protocols and a constant Fe : P ratio of 1 : 100. Prior to incubations, minerals were pelleted by centrifugation to remove free P (Supporting Information Note 2). Due to the overlap in the energies of both isotopes we did not synthesize double-labeled minerals, but signal separation is possible if other isotopes of P or Fe are used.

#### Phosphate dissolution rates

Rates of mineral dissolution or  $^{33}\text{P}$  release were studied in trace metal clean 15-mL tubes filled with sterilized filtered seawater (FSW) in the absence of cells and were typically conducted in duplicates. All treatments were kept at  $25^\circ\text{C}$  under shaking for 15–20 h. Aliquots were collected over time and filtered using a  $0.22\text{-}\mu\text{m}$  (Pall, Acrodisc) syringe filter. The radioactive filtrate was collected in scintillation vials, mixed with Quick-Safe scintillation cocktail, and measured in a Tri-carb 1600 CA (PerkinElmer, Packard). In each experiment we also recorded the initial fraction of dissolved  $^{33}\text{P}$ . For the  $^{33}\text{P}$ -adsorbed ferrihydrite, the initial dissolved P fraction was significant (9–65%), and its  $^{33}\text{P}$  desorption rate was rather high,  $5\% \pm 3\%$  per hour (Table 1). Subsequently, these assays contained high dissolved  $^{33}\text{P}$  concentrations, deeming the  $^{33}\text{P}$ -adsorbed ferrihydrite unsuitable for studying bioavailability of particles. Elevated dissolved  $^{33}\text{P}$  was also recorded when the coprecipitated Fe- $^{33}\text{P}$  ferrihydrite was added to seawater. Based

**Table 1.** Characterization experiments of the two synthesized Fe- $^{33}\text{P}$  minerals. Two features were tested, the initial partitioning of P between dissolved and particulate phases, and the P dissolution/desorption kinetics.

Mineral type	Initial partitioning		Dissolution/desorption kinetics		
	Dissolved P	Particulate	Rate	Constant	Constant
	%	%	$\text{nM d}^{-1}$	$k_{\text{diss}} (\text{d}^{-1})$	% per hour
(A) $^{33}\text{P}$ adsorbed on ferrihydrite					
17 Oct 2018	36	64	1.2	0.2	1
28 Oct 2018	9	91	12.8	2.3	10
18 Mar 2019	65	35	12.5	1.3	5
18 Mar 2019	15	85	3.3	1.5	6
			Average	$1.3 \pm 0.9$	$5 \pm 4$
(B) $^{33}\text{P}$ co-precipitated as Fe-P mineral					
11 Apr 2019	2	98	0.30	0.04	0.2
29 Apr 2019	4	96	0.25	0.04	0.1
			Average	$0.04 \pm 0.01$	$0.2 \pm 0.0$

on the assumption that this P was not incorporated but loosely adsorbed on the mineral surfaces, this fraction was removed by applying repeated washes. The wash procedure involved three spin-down cycles of the mineral at 2000 rpm (1 h each) followed by a resuspension of the pellet in filtered SW. Based on the  $^{33}\text{P}$  fraction measured in the supernatant, the three wash-steps removed about 25–30% of the added P. Following this treatment, most batches of coprecipitated Fe- $^{33}\text{P}$  ferrihydrite had a negligible initial dissolved P fraction (Table 1). During the assay, the  $^{33}\text{P}$  release rate was moderate (0.1–0.2% per hour), making the coprecipitated Fe- $^{33}\text{P}$  ferrihydrite a good model for mineral-phase P availability studies (Table 1).

It should be noted, however, that our synthesis of radiolabeled minerals was simplified compared to the classical procedures described by Schwertmann and Cornell (2008), and resulted in variations among batches. Phosphate is more soluble than Fe and occasionally we observed rapid release of  $^{33}\text{P}$  also from the washed co-precipitated mineral (Supporting Information Note 1; Tables S1, S2). It is hence important to characterize the dissolution/release kinetics of the synthesized mineral prior to each experiment. For simplicity, we refer to these minerals as  $^{33}\text{P}$ -labeled ferrihydrite for the rest of the paper.

### **Trichodesmium collection, handling, and culturing** **Natural Red Sea Trichodesmium colonies**

Puff-shaped colonies of *Trichodesmium thiebautii* (Koedooder et al. 2022) were collected by net-tows from the Gulf of Eilat/Aqaba during springs 2019 and 2022. The colonies were quickly hand-picked from the net-concentrate under a stereoscope using plastic droppers and were suspended in a petri dish with FSW. Integral and well-formed colonies were then selected for the uptake assays and rinsed by 3–5 repeated transfers to new FSW. Finally, 30–50 colonies were placed in a petri dish and maintained at 25°C with a light intensity of  $\sim 80 \mu\text{mol photons m}^{-2} \text{s}^{-1}$ . On one occasion in spring 2019, tuft-shaped colonies of *Trichodesmium erythraeum* (Koedooder et al. 2022) were collected and treated in a similar way. Images of selected colonies were obtained using a camera attachment to a stereoscope for assessing interactions with the added radiolabeled minerals.

### **T. erythraeum strain IMS101 culture**

A culture of *T. erythraeum* strain IMS101 was grown at 25–26°C, 12 : 12 h photoperiod at  $\sim 80 \mu\text{mol photons m}^{-2} \text{s}^{-1}$  in a modified YBC-II medium that contained 20  $\mu\text{M}$  ethylenediaminetetraacetic acid (EDTA). Cultures were grown on 5  $\mu\text{M}$  phosphate that in the late exponential phase leads to mild P-limitation. This mild P-limitation resulted in reduced final biomass (detected by in vivo fluorescence and cell counts) and lengthening and thinning of the trichomes (Mulholland et al. 2002). Prior to uptake assays, 200–300 mL of culture was gravity filtered on polycarbonate filters (8  $\mu\text{m}$ ,

$\varnothing$  47 mm, Nuclepore©) and rinsed five times with FSW. Filament (trichome) enumeration for strain IMS101 involved fixation with Lugol's solution and manual counting using a Sedgwick-Rafter Cell (Pyser-SGI) under bright-field Nikon Eclipse Ci-E microscope, at 10 $\times$  magnification. The numbers of trichomes in the natural colonies were repeatedly counted on tens of colonies (see also Basu and Shaked 2018). Counting was done on images of intact colonies and/or colonies that were separated into single filaments by shaking.

### **Uptake assays from $^{33}\text{P}$ -labeled ferrihydrite** **Setup and assay initiation**

Uptake assays with natural colonies were carried out in petri dishes ( $\varnothing$ 15 mm) filled with  $\sim 2$  mL FSW at a density of  $\sim 15$ –25 puffs  $\text{mL}^{-1}$ . Cultured strain IMS101 was placed in small Nalgene bottles filled with 10–30 mL P-free YBC-II media at a density of  $\sim 1.5$ –2.5  $\times 10^4$  trichomes  $\text{mL}^{-1}$ . Experiments were initiated by pipetting 7–20 nM  $^{33}\text{P}$ -labeled ferrihydrite directly on natural colonies or concentrated culture trichomes, to ensure optimal cell–mineral associations and avoid mineral loss to the container walls. To further favor cell–mineral contact, cells were maintained initially in 0.5–1 mL, and the remaining water was added once the interaction was visually confirmed in a stereoscope (Fig. 1). Colonies were then incubated with the mineral for 3–8 h at 25°C under illumination ( $\sim 80 \mu\text{mol photons m}^{-2} \text{s}^{-1}$ ). Uptake assays with cultured *Trichodesmium* (IMS101) were conducted in duplicates. Due to biomass limitation, uptake assays with natural colonies were typically not replicated on a single day but were conducted repeatedly over several days

### **Cell harvesting and removal of external P**

The extracellular  $^{33}\text{P}$  associated with minerals was removed using a Ti–EDTA–citrate solution that reductively dissolved ferrihydrite (Hudson and Morel 1989). Following Basu and Shaked (2018), Ti–EDTA–citrate wash was added directly to the cells (3 : 1 volumetric ratio of wash to FSW) and the mixture was incubated for 25 min. Colonies were then gravity filtered on 8- $\mu\text{m}$  polycarbonate filter, rinsed thrice with 1 mL of FSW, and counted in liquid scintillation counter. This procedure replaces the standard 10 min wash of cells on filters, which was found insufficient to remove all minerals. Uptake assays with glutaraldehyde-killed colonies using both bulk scintillation counting and beta-imaging confirmed that this procedure indeed removed all external P (Fig. 1). We also confirmed that P did not leak from the cells due to the washes (Supporting Information Note 3).

### **Effect of desferrioxamine B on P dissolution and uptake**

Following the above method, we next probed for the effect of the microbially produced siderophore desferrioxamine B (DFB) on abiotic dissolution of  $^{33}\text{P}$ -labeled ferrihydrite ( $\sim 7$  nM P) in seawater, and on cellular uptake of both natural colonies and cultured *Trichodesmium*. DFB was added at a final concentration of 1–2  $\mu\text{M}$  in our incubations, with seawater

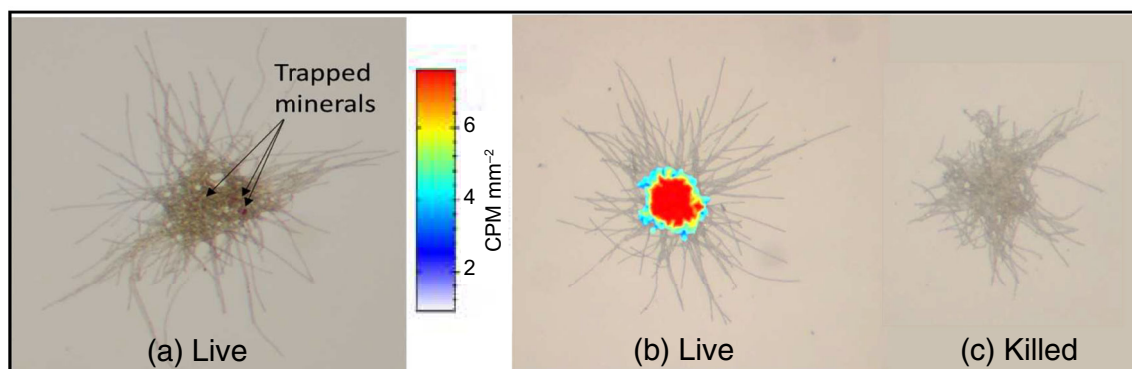


**Fig. 1.** Method verification: colony-particle interactions, removal of external mineral and  $^{33}\text{P}$  internalization. **(a)** Microscopic image of a colony that trapped Fe-P particles (not washed). **(b,c)** Beta-imaging maps of  $^{33}\text{P}$  overlaid upon microscopic images of colonies incubated with 7 nM  $^{33}\text{P}$ -labeled ferrihydrite for 12 h and washed with Ti-EDTA-citrate to remove external  $^{33}\text{P}$ . Uptake of  $^{33}\text{P}$  is seen in the center of the live colony **(b)**, while the efficiency of the wash in removing all external  $^{33}\text{P}$  is evident from the lack of radioactivity in the killed colony **(c)**.

serving as controls. In order to confirm that the added DFB was not inhibiting the P acquisition, we also studied the effects of added DFB on cellular uptake of dissolved inorganic  $^{33}\text{P}$  (Supporting Information Fig. S2).

#### Radioimaging of $^{33}\text{P}$ uptake by single colonies

As in the “bulk” uptake experiments,  $^{33}\text{P}$ -labeled ferrihydrite containing 7–10 nM P was mixed with fresh puff-shaped colonies and incubated for 3–7 h. Then, colonies were gently soaked in Ti-EDTA-citrate solution to ensure complete removal of external  $^{33}\text{P}$ , rinsed individually by three serial washes in FSW using a plastic dropper, and finally soaked in 1% paraformaldehyde (PFA) to remove the salt crystals. Colonies were placed on poly-L-lysine-coated glass slides and left to air dry. Separate slides were prepared for the killed controls (Fig. 1). Prior to imaging, slides were covered with 10- $\mu\text{m}$ -thick scintillation foil and imaged in a BetaImager<sup>™</sup> (Biospacelab) until 2 million counts were reached. The images were analyzed for counts per minute (CPM) per colony and the spatial distribution of radioactivity was recorded (Biospacelab, M3Vision). Total uptake per colony was calculated from the specific activity of the mineral ( $1.52 \times 10^{15}$  CPM mol<sup>-1</sup>) multiplied by 2, as the foil captures only half of the radiation. Due to short half-life of  $^{33}\text{P}$ , all radioactive counts were corrected for decay.

#### Effects of superoxide on mineral dissolution and uptake by *Trichodesmium*

In spring 2022, a series of dissolution and uptake experiments were conducted with P-ferrihydrite labeled with either  $^{33}\text{P}$  or  $^{55}\text{Fe}$  and cultured strain IMS101. Superoxide ( $\text{O}_2^-$ ) was generated by dissolving ~10–25 mg of  $\text{KO}_2$  in pH 12.5 trace-metal-cleaned NaOH solution (Diaz et al. 2013). Absorbance was immediately recorded in an UV/Vis spectrophotometer at 240 nm, with and without additions of superoxide dismutase (SOD, 10 U mL<sup>-1</sup>). Since, SOD dismutates  $\text{O}_2^-$  to generate

$\text{H}_2\text{O}_2$ , the final molar concentration of  $\text{O}_2^-$  in the stock was calculated following molar absorptivity corrections for  $\text{H}_2\text{O}_2$  (Bielski et al. 1985). The stock solutions were diluted to a pH 8 NaOH solution and then added to the incubations, targeting a concentration of ~100 nM  $\text{O}_2^-$ . Since  $\text{O}_2^-$  decays rapidly in seawater (half-life of few minutes), the actual  $\text{O}_2^-$  concentrations added are expected to be lower. The actual  $\text{O}_2^-$  concentrations were not recorded during the ~6 h uptake or dissolution assay due to volume restrictions. Instead,  $\text{O}_2^-$  was added at regular intervals of 1.5 h.

## Results

### Uptake and dissolution rates of phosphate from Fe- $^{33}\text{P}$ minerals

We applied our method to determine rates of phosphate dissolution (abiotically) and uptake from  $^{33}\text{P}$ -labeled ferrihydrite by both, field-collected colonies and laboratory cultured *Trichodesmium*. The first set of experiments was conducted during April and May 2019 with natural Red Sea colonies from two different species, namely *T. thiebautii* (puff-shaped colonies) and *T. erythraeum* (tuft-shaped colonies) (Koedooder et al. 2022). In parallel, we tested also the ability of P-limited *Trichodesmium* cultures (strain IMS101) to acquire phosphate from  $^{33}\text{P}$ -labeled ferrihydrite and followed the rate of phosphate dissolution from the mineral in the absence of cells. To enable comparison among experiments, rates were normalized to the number of trichomes (filaments) present in each experiment.

Trichome-normalized uptake rates varied by up to fourfold, with puff-shaped colonies showing higher rates than tuft-shaped colonies and P-limited cultures (Fig. 2a). Such variations in P uptake rates may reflect differences in cell-particle interactions. Iron uptake from ferrihydrite was shown to be linked to colony-particle interactions (Rubin et al. 2011; Basu and Shaked 2018). Likewise, the lower P uptake by the single trichomes of IMS101 (Fig. 2a) may result from their weaker

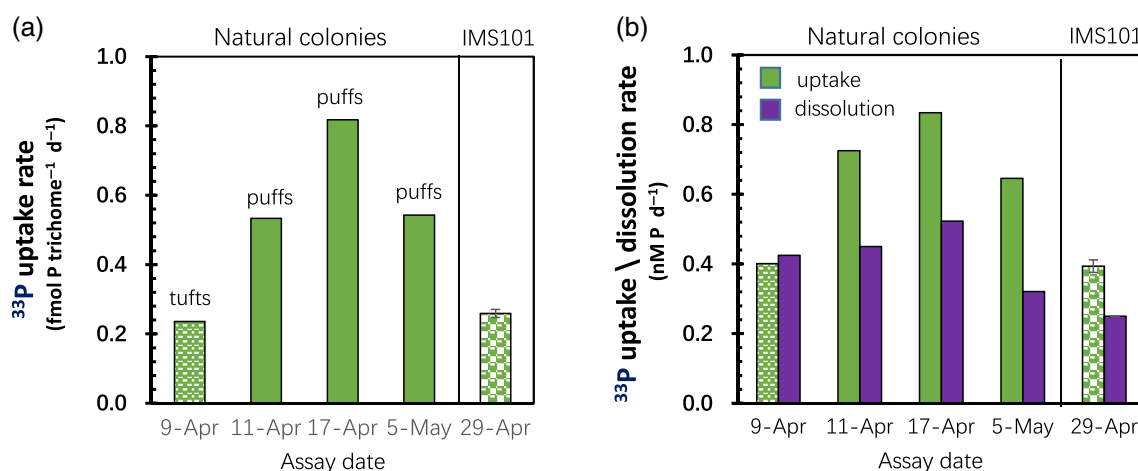


**Fig. 2.** Phosphorus uptake rates from  $^{33}\text{P}$ -labeled ferrihydrite by cultured and natural *Trichodesmium* colonies, collected from the Gulf of Aqaba on different days. **(a)** Uptake rates normalized to trichomes (i.e., biomass normalized), for comparison among species. **(b)** Total uptake rates (green bars) extended together with phosphate dissolution rates from  $^{33}\text{P}$ -labeled ferrihydrite (purple bars). Dissolution rates measured in the absence of cells, provide a measure for the P supply from the minerals. Same uptake experiments are shown in both panels but the data is calculated differently, allowing interspecies comparison **(a)** and uptake and dissolution rates comparison **(b)**. Rates of uptake by cultures are duplicated, while low biomass prevented replication of uptake by natural colonies.

interactions with particles compared with the intricate puff-shaped colonies (Kessler et al. 2020a). Yet, the interspecies variations in mineral P uptake are less pronounced than those of mineral Fe (Rubin et al. 2011; Basu and Shaked 2018), probably due to the higher solubility of the P-minerals (Table 1; Supporting Information Table S1). Phosphorus uptake rates may also be affected by the organism's P nutrition. Natural Red Sea *Trichodesmium* spp. were shown to experience P limitation based on P stress marker genes (Wang et al. 2022) and alkaline phosphatase activity (Stihl et al. 2001). Here, we did not assess directly the colony's P stress, but the high uptake signal obtained from only several colonies suggests that natural colonies are in a need for P and hence express their high affinity P transport systems.

Next, we compare the overall phosphate uptake rates with the mineral P release/dissolution rates, which were determined in parallel without cells. Since *Trichodesmium* internalizes only dissolved P, the overall uptake rate is indicative of the dissolved P flux to the cells. Efficient uptake of all P released from the mineral will result in similar dissolution and uptake rates. Faster uptake than dissolution implies cell-mediated dissolution, while slower uptake than dissolution hints at some constrain for utilization. As expected, dissolution rates of  $^{33}\text{P}$ -labeled ferrihydrite in cell-free seawater were rather constant among days, ranging from 0.3 to 0.5 nM P d $^{-1}$  (Fig. 2b). These rates represent dissolution of 0.2–0.3% of the P in the mineral per hour, as seen in our characterization experiments (Table 1). The overall P uptake by *Trichodesmium* in each of these days was similar or higher than P dissolution rate (Fig. 2b). For Fe, rates of  $^{55}\text{Fe}$  uptake repeatedly exceeded  $^{55}\text{Fe}$  ferrihydrite dissolution by up to threefold, demonstrating that natural *Trichodesmium* colonies actively promote

ferrihydrite dissolution (Basu and Shaked 2018). Here, the limited number of experiments and the small excess of uptake over dissolution are not sufficient to confirm biotically induced/mediated dissolution of phosphate from iron minerals. Further research examining the ability of the *Trichodesmium* consortium to solubilize P from minerals is required.

### Single colony uptake of P from $^{33}\text{P}$ -labeled ferrihydrite

The uptake experiments presented so far were conducted with 20–50 colonies that were collected on a single filter and measured with a scintillation counter. This technique provides quantitative information on the bulk uptake of all colonies present in the assay, but is not sensitive enough for analyzing single colony uptake. Hence, we also studied P uptake from  $^{33}\text{P}$ -labeled ferrihydrite by individual natural colonies using 2D beta-imaging. We consider this method as complementary to the standard uptake assays, allowing a closer look into colony–colony variations and localization of the internalized P. This technique enabled us to validate that all external particulate  $^{33}\text{P}$  was efficiently washed from the colonies (Fig. 1). In addition, light microscopy revealed that all colonies remained intact after washing and fixing the cells (see “Effect of desferrioxamine B on P dissolution and uptake” section), and that the size and morphology of the colonies differed (Fig. 3a, bottom panel). Beta-imaging of these colonies showed high variability in the  $^{33}\text{P}$  signal among colonies, indicating that some colonies acquired relatively high P, while others did not internalize any P (Fig. 3a, top panel). This intriguing finding points to the importance of cell–mineral proximity for uptake and may hint at a role of the colony microbiome in increasing mineral P bioavailability. Furthermore, beta-

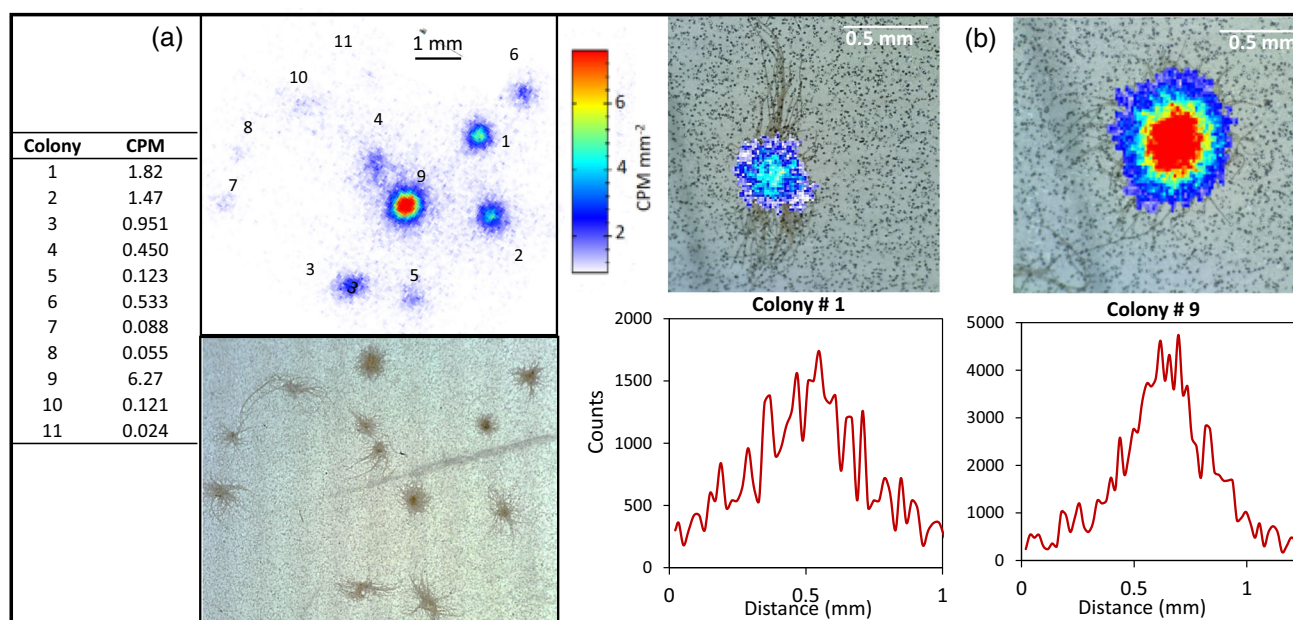


**Fig. 3.** Radioimaging of  $^{33}\text{P}$  uptake of natural *Trichodesmium thiebautii* colonies from  $^{33}\text{P}$ -labeled ferrihydrite. **(a)** Microscopic and radioimages of colonies on a slide. **(b)** Representative light microscope images of colonies overlaid with radioimages (top panel) and distribution of radioactivity counts along spatial transects through the center of the colony (bottom panel).

imaging was applied to obtain spatial information on uptake at subcolony resolution. In accord with our former study using  $^{55}\text{Fe}$  ferrihydrite (Basu et al. 2019), overlaying  $^{33}\text{P}$  distribution maps of single colonies on their microscopic images yielded a  $^{33}\text{P}$  signal localized in the colony center (Fig. 3b, upper panel). This intense  $^{33}\text{P}$  signal in the colony core may originate from high cell–mineral proximity and lower diffusive losses of P, but may also reflect the high density of filaments in the colony core. Cross sections of the colonies reveal fivefold to eightfold higher  $^{33}\text{P}$  accumulation in the colony's center compared to its periphery (Fig. 3b, lower panel). Density changes of twofold to sevenfold estimated from the images, leave both interpretations plausible. Hence, the higher  $^{33}\text{P}$  uptake observed in the colony core (Fig. 3b) may originate from particle–cell proximity and minimized diffusive losses of the P released from the mineral, but may also reflect higher cell density.

### Pathways inducing ferrihydrite dissolution and subsequently increasing P availability

In oceanic settings, P containing Fe minerals (generally noted as P-bound Fe), are next in abundance to apatite (Paytan and McLaughlin 2007; Duhamel et al. 2021). Hence, reactions leading to dissolution of Fe minerals increase P release and thus enhance availability to microbes. Common microbial pathways for solubilizing Fe minerals include ligand-assisted and reductive dissolution, which are often activated under Fe-limiting conditions (Melton et al. 2014; Kappler et al. 2021). Interestingly, P-limitation can also

activate these pathways. For example, upon P-limitation some marine bacteria were found to synthesize molecules, which were identified as siderophores (strong Fe-binding ligand, Romano et al. 2017). Here, we examined whether a siderophore (DFB) and a reductant (superoxide) can enhance: (a) ferrihydrite dissolution rate, (b) P release rate, (c) Fe uptake rate, and (d) P uptake rate. Our experimental approach involved synthesizing  $^{33}\text{P}$ -Fe and P- $^{55}\text{Fe}$  ferrihydrite and conducting uptake and cell-free dissolution assays with these reactants.

Starting with siderophores, we chose DFB, which we detected during in situ *Trichodesmium* blooms and short-term incubations (Basu et al. 2019; Gledhill et al. 2019). We first confirmed that 1–2  $\mu\text{M}$  DFB indeed enhance Fe dissolution using P-ferrihydrite labeled with  $^{55}\text{Fe}$  (Fig. 4a). These concentrations exceed those detected in natural blooms, but may reflect concentrations in the colony core (Kessler et al. 2020b). Next, we tested the effect of DFB on P release from  $^{33}\text{P}$ -labeled ferrihydrite in the absence of cells, and on P uptake by natural and cultured *Trichodesmium*. In all experiments, the addition of DFB accelerated  $^{33}\text{P}$  release and resulted in faster P uptake rates (Fig. 4b,c; Supporting Information Tables S4, S5). Interestingly, the effect of DFB on P dissolution was stronger (twofold to sevenfold enhancement; Fig. 4b) than its effect on P uptake (1.1- to 1.6-fold enhancement, Fig. 4c), indicating that some of the DFB-released P was not internalized by the cells. This is in contrast to  $^{55}\text{Fe}$ , where DFB quantitatively enhanced dissolution and uptake from  $^{55}\text{Fe}$  ferrihydrite (Basu et al. 2019). An inhibitory effect of DFB on *Trichodesmium*'s P uptake system was ruled out by conducting experiments with dissolved  $^{33}\text{P}$ ,

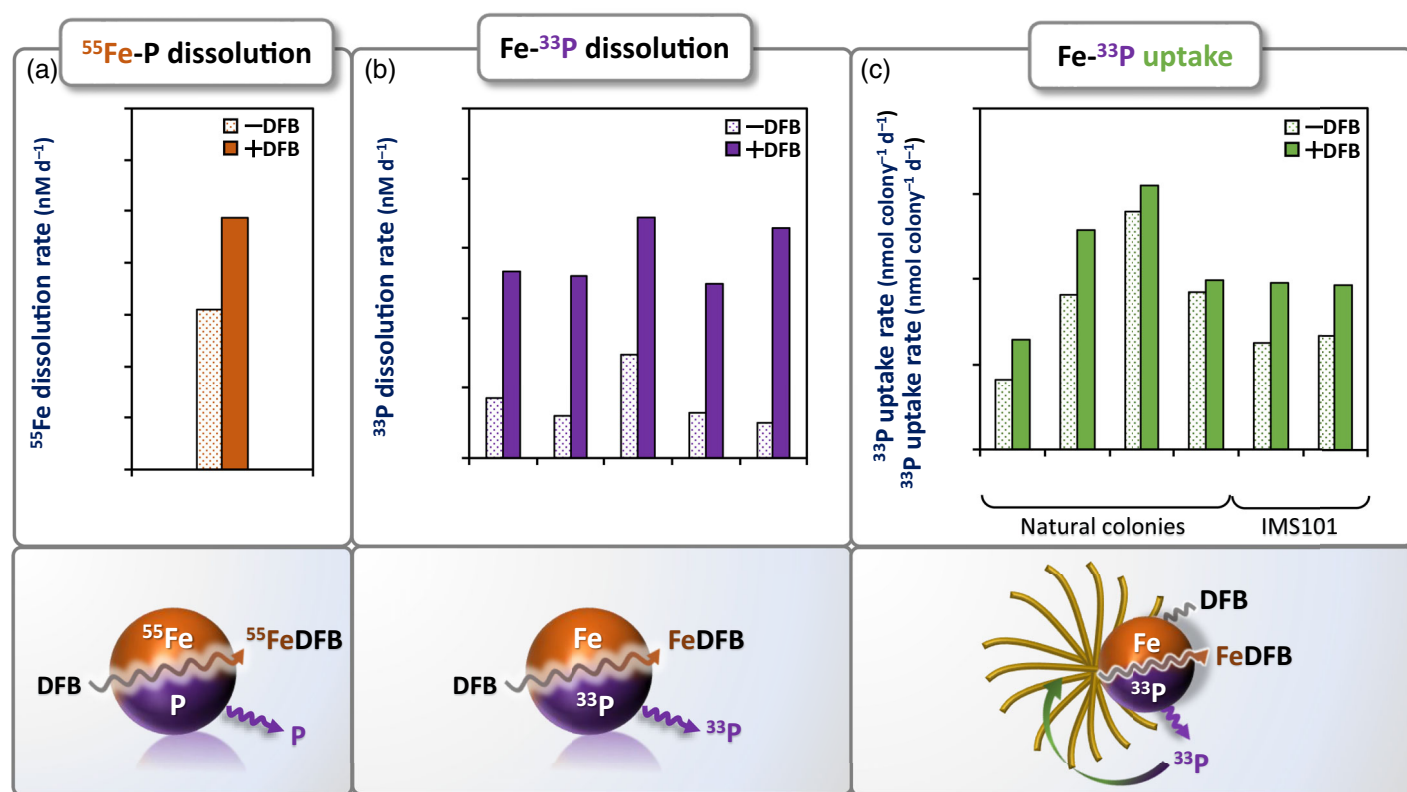


**Fig. 4.** Effect of the Fe-binding ligand DFB on Fe and P release from Fe-P minerals and P uptake by P-limited *Trichodesmium erythraeum* (strain IMS101). (a) DFB enhances  $^{55}\text{Fe}$  release from P- $^{55}\text{Fe}$ -ferrihydrite. (b) DFB enhances  $^{33}\text{P}$  release from  $^{33}\text{P}$ -ferrihydrite. (c) DFB enhances  $^{33}\text{P}$  uptake from  $^{33}\text{P}$ -ferrihydrite. Cartoons under each graph schematically represent the major reactions. Rates of uptake by cultures are duplicated, while low biomass prevented replication of uptake by natural colonies.

showing comparable uptake rates with and without DFB (Supporting Information Fig. S2). Hence the weaker P-uptake response observed here may reflect faster diffusive loss of the small P molecule ( $^{33}\text{PO}_4$ ) released by DFB compared to the “bulky”  $^{55}\text{Fe}$ -DFB complex.

Turning to superoxide ( $\text{O}_2^-$ ), a reactive oxygen species, which is produced and released to seawater by natural *Trichodesmium* colonies under physiological conditions (Hansel et al. 2016). An involvement of  $\text{O}_2^-$  in Fe uptake by several cyanobacteria was documented under oxic conditions, where  $\text{O}_2^-$  catalyzes reductive dissolution of high labile Fe minerals (Rose et al. 2005; Swanner et al. 2015). Here we seek to extend these findings and test if externally added  $\text{O}_2^-$  can also enhance  $^{33}\text{P}$  release rate and  $^{33}\text{P}$  uptake. Since  $\text{O}_2^-$  is highly reactive, capable of reducing and oxidizing Fe and additional metals and can even react with itself (dismutate), it is hard to experimentally control this system (Morris et al. 2022). Moreover, given the low solubility of Fe in seawater, Fe may quickly reprecipitate, possibly along with  $^{33}\text{P}$  (Gunnars et al. 2002). We hence repeated the assays many times adding  $\text{O}_2^-$  (as  $\text{KO}_2$ ) at different intervals and

concentrations. We also tested several types of P-ferrihydrite, synthesized according to different protocols and varying in their P release rates (Supporting Information Table S2).

A positive effect of  $\text{O}_2^-$  on Fe dissolution and uptake by cultured *Trichodesmium* was found for  $^{55}\text{Fe}$ -labeled P-ferrihydrite (Fig. 5a; Supporting Information Table S4). Yet, the effect of  $\text{O}_2^-$  on P release and uptake from  $^{33}\text{P}$ -ferrihydrite was less consistent (Fig. 5b; Supporting Information Table S3). We chose to show all data, presenting the rate ratio of experiments with added  $\text{O}_2^-$  over the control, for both P release and P uptake (Fig. 5b). A large scatter in the data is seen, with ratios close to 1 (no effect), lower than 1 (negative effect), and higher than 1 (positive effect). This scatter can be partly explained by the six different  $^{33}\text{P}$ -ferrihydrite batches used, noted by distinct symbols (Fig. 5b). For some of these minerals, primarily those utilized in the beginning, a positive effect of  $\text{O}_2^-$  on P uptake and release was detected. To conclusively show a positive effect of  $\text{O}_2^-$  on P dynamics, a fine-tuning of the mineral synthesis and  $\text{O}_2^-$  generation is required. Overall, based on our data (Fig. 5), we conclude that  $\text{O}_2^-$  can enhance Fe (and possibly also P) release and uptake.

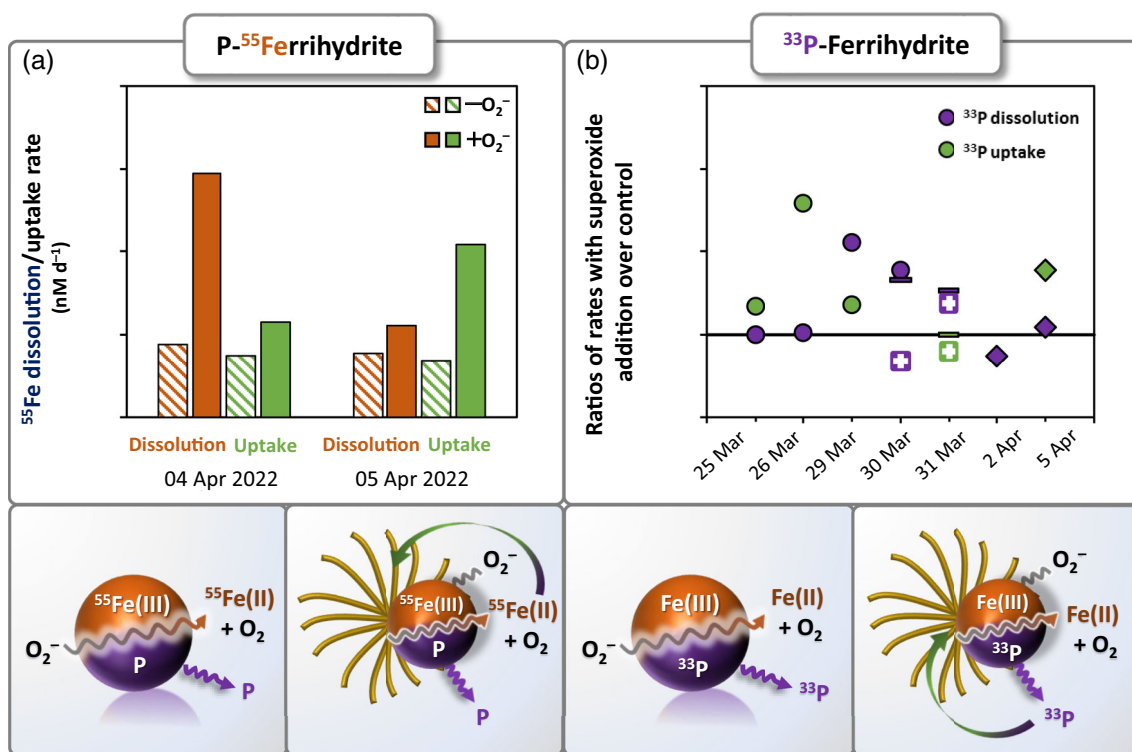


**Fig. 5.** Effect of superoxide ( $\text{O}_2^-$ ) on Fe and P release from Fe-P minerals and uptake by P-limited *Trichodesmium erythraeum* (strain IMS101). **(a)** Superoxide enhances  $^{55}\text{Fe}$  release and uptake from P- $^{55}\text{Fe}$ ferrihydrite. **(b)** Superoxide enhances  $^{33}\text{P}$  release and uptake from  $^{33}\text{P}$ -ferrihydrite. Dissolution or uptake data are presented as ratios of rates with added superoxide over control. Symbols represent the different minerals tested. Cartoons under each graph schematically represent the major reactions. Raw data are presented in Supporting Information Tables S3 and S4.

## Discussion

### Analytics of Fe- $^{33}\text{P}$ mineral uptake

One of the largest challenges in studying availability of particulate nutrients is to separate the small signal of internalized nutrient from the large signal of external particles, while maintaining the organism integrity. We chose to use Fe-minerals (here ferrihydrite) as the scaffold for particulate P, since Fe-minerals were found to undergo complete reductive dissolution and complexation with Ti-EDTA-citrate wash, providing a method to remove all external P (Hudson and Morel 1989; Tang and Morel 2006; Basu and Shaked 2018). We synthesized two Fe-minerals labeled with radioactive  $^{33}\text{P}$ : (a)  $^{33}\text{P}$ -adsorbed ferrihydrite and (b)  $^{33}\text{P}$ -labeled ferrihydrite (based on co-precipitation). The first released too much  $^{33}\text{P}$  into solution, so that the assay was in fact predominantly a dissolved P assay (Table 1), and hence this mineral was not used further. The  $^{33}\text{P}$ -labeled ferrihydrite provided a slow and steady flux of dissolved P and supported measurable uptake (Table 1; Fig. 2). Microscopic- and beta imaging confirmed efficient removal of external mineral-phase and adsorbed  $^{33}\text{P}$ , mineral centering by the colonies, and elevated  $^{33}\text{P}$  uptake in the colony core (Fig. 1; Supporting Information Table S1). We also confirmed that the Ti-EDTA-citrate wash did not cause

leakage of intracellular P (Supporting Information Note 3). Furthermore, this setup allows examining Fe bioavailability in parallel by synthesizing  $^{55}\text{Fe}$ -P minerals as shown in Figs. 4, 5.

Overall, our study successfully addressed many challenges related to measuring uptake from minerals, ensuring high sensitivity, rapid detection, parallel measurements of mineral dissolution (or release) kinetics, and effective removal of minerals from cells. Nonetheless, we encountered several inherent problems. For example, the 2D imaging uncovered that single colony uptake of  $^{33}\text{P}$  from minerals is highly heterogeneous (Fig. 3), probably due to different degree of colony-mineral interactions and physiological diversity in the colony's microbial community. Yet, bulk  $^{33}\text{P}$  uptake values for replicate samples obtained for different days remained relatively stable (Fig. 2), indicating sufficient homogenization of the colonies for bulk measurements. Thus, we recommend future studies to consider the degree of colony-particle interaction, as it is a key feature for uptake. We also encountered difficulties during mineral synthesis, since only a small fraction of  $^{33}\text{P}$  was incorporated into the precipitate (< 10% mol), as reported by Kraal et al. (2020). Subsequently, a large fraction of the  $^{33}\text{P}$  was adsorbed onto the mineral surface and thus easily released during the experiments. Yet, we managed to remove this

fraction by applying three washing steps prior to experiment (Supporting Information Note 2). Acknowledging differences among discrete mineral batches, we synthesized (Supporting Information Note 1; Table S2), care should be practiced when comparing results from our two field seasons.

Despite these short-comings, our methodology enabled us to link rates of Fe-P mineral dissolution and uptake by natural *Trichodesmium* colonies (Fig. 2), examine P uptake by individual colonies (Fig. 3) and experimentally demonstrate the potential of reductive and ligand assisted dissolution to co-extract Fe and P from particles (Figs. 4, 5), such as aerosols or re-suspended sediments. Our method and novel concepts build upon and feed into a growing appreciation of the prevalence of microbe–particles interactions and microbial mineral-transformations in different ocean ecosystems throughout the water column (Azam and Malfatti 2007; Seymour et al. 2017).

### Implications for *Trichodesmium*'s Fe and P nutrition

Most research on P uptake of *Trichodesmium* focused on its versatile and unique abilities to obtain P from organic sources (Dyhrman et al. 2006). To the best of our knowledge, our data on bulk and single colony phosphate uptake from solid-phase P (Figs. 1–5) are the first of their kind. Our study also highlights a mostly unexplored link between Fe and P uptake, which we title co-acquisition. This co-occurring uptake results from bio-dissolution mechanisms acting on both Fe and P that are often in close geochemical association in soils, sediments and aerosols. Although apatite is the most common P mineral, its low solubility renders it poorly bioavailable in natural waters (Duhamel et al. 2021). The next largest particulate P pool is P-bound Fe, a poorly defined heterogenous pool, composed of authigenic minerals that form during weathering, transport and within sediment redox boundaries (Paytan and McLaughlin 2007; Egger et al. 2015). When *Trichodesmium* spp. interact with P-bound Fe particles they may benefit from co-release of both nutrients. Moreover, when the colony's microbiome “mine” minerals for dissolved Fe, they may further benefit from co-release of bioavailable phosphate (Figs. 4, 5). Several new studies, suggesting that P-limited bacteria produce ligands or redox reactive antibiotics that can solubilize Fe-minerals and foster P release, further support these ideas (Romano et al. 2017; McRose and Newman 2021; Cui et al. 2022). Our findings are relevant to many ocean regions, such as the North Atlantic Gyre, where *Trichodesmium* populations are co-limited by Fe and P (Held et al. 2020; Cerdan-Garcia et al. 2022). Surprisingly, *Trichodesmium* spp. can optimize their performance to thrive specifically under Fe-P co-limitation, reaching higher growth than under only Fe or P limitation (Walworth et al. 2016). Intriguing laboratory and field investigations identified a unique molecular signature indicating physiological remodeling, enabling *Trichodesmium* spp. to adapt and exploit an Fe-P co-limited ocean niche (Walworth et al. 2016; Held et al. 2020; Cerdan-Garcia et al. 2022). It is possible that the co-occurring uptake

of Fe and P from minerals offers an additional adaptation to this niche.

There are also differences among these elements, especially regarding dissolution (or desorption) and metabolic requirements. Comparing rates of  $^{55}\text{Fe}$  and  $^{33}\text{P}$  dissolution in the current and past studies (Basu and Shaked 2018; Basu et al. 2019), reveal larger fluxes of  $^{33}\text{P}$  from the ferrihydrite compared to  $^{55}\text{Fe}$  (Supporting Information Tables S1, S3, S4). The elevated  $^{33}\text{P}$  release likely results in higher loss by diffusion from the colonies, possibly explaining the moderate effect of DFB and superoxide on  $^{33}\text{P}$  uptake (Figs. 4, 5). Despite its higher solubility, inorganic particles (aerosols, suspended sediments) are typically considered negligible source of P compared to Fe (Moore et al. 2013). This is so, since *Trichodesmium*'s P requirements are 10–100 higher than those of Fe (Dyhrman 2016), while most aerosols contain more Fe than P (Anderson et al. 2010). Bearing in mind the importance of multiple organic P sources utilized by *Trichodesmium* and its associated microbiome (Frischkorn et al. 2017), we suggest it is important to consider P supply from (some) inorganic particles.

### Extending our views on particles bioavailability to phytoplankton

Next, we zoom-out and explore the broader topic of particulate nutrients bioavailability to phytoplankton. In the context of marine primary productivity, a strong emphasis is placed on evaluating and modeling nutrient fluxes from aerosols (e.g., ash or eolian dust) deposited on the ocean surface (Mahowald et al. 2018). With regards to P release and bioavailability after aerosol deposition, it is commonly assumed to be controlled by P speciation in the aerosol (Shi et al. 2019; Dam et al. 2021). But also in the seawater P availability can be altered, by organic ligands, phytoplankton and/or bacteria.

Seawater composition was shown to effect aerosol Fe solubility, by means of reductive or ligand assisted dissolution (Aguilar-Islas et al. 2010). As shown here experimentally (Figs. 4, 5), such pathways can also enhance P release. Microbes residing in seawater, either alive or degraded, can further affect the aerosol solubility by physically attaching to aerosols and hence alter their residence time in the ocean surface. Cell–particle interactions are commonly reported in lakes and coastal regions, but even in remote ocean regions there are indications for such encounters (Held et al. 2021; Dansie et al. 2022). Cell–particle interactions can strongly affect the particle fate and chemical *milieu* and subsequently change its solubility and bioavailability. Mineral–cell interactions and bio-modifications of Fe–minerals were reported for several phytoplankton including coastal and marine cyanobacteria (Rose et al. 2005; Kranzler et al. 2016; Swanner et al. 2018), and diatoms (Hettiarachchi et al. 2021).

In the case of *Trichodesmium*, the colony microenvironment enables reactant build-up and minimizes diffusive losses, and thus favors mineral dissolution and uptake (Rubin

et al. 2011; Basu and Shaked 2018; Eichner et al. 2020). Ligand-assisted mineral-Fe dissolution proceeds through mutualistic interactions among the microbes composing the colony consortium (Basu et al. 2019), where bacteria synthesize siderophores that solubilize Fe minerals, while *Trichodesmium* provides fixed carbon and nitrogen essential for siderophore synthesis (Gledhill et al. 2019). Such ligand-promoted dissolution may also enhance solubility and availability of P associated with Fe-mineral, as we show here (Fig. 4). Other pathways for increasing P fluxes include reductive dissolution of Fe-minerals, via superoxide (Fig. 5; Hansel et al. 2016) and additional reductases released by *Trichodesmium* and its associated bacteria.

In light of the multiple pathways by which *Trichodesmium* and additional phytoplankton species employ for altering aerosol Fe (and likely P) solubility, we propose to extend our view on the availability of particulate nutrients, and reclaim the term “bio” in bioavailability. We place the chemical solubility of the aerosol as the basis of this bioavailability scheme, typically evaluated by standard leaching techniques using seawater, distilled water or weak acids (Perron et al. 2020). We then suggest to add another component related to physical attachment between cells and particles that can optimize nutrient supply to the cell. This optimization results from longer nutrient release time in the immediate proximity to the cells. Finally, we offer to augment the role of biologically mediated modifications in increasing bioavailability. Such modifications, even if subtle, can lead to elevated fluxes, given time and cell-particle proximity. Thus, biological processes prevailing in marine microhabitats likely affect marine biogeochemical cycles on a large scale and should be considered when referring to particle and/or aerosol-derived nutrient bioavailability in marine environments.

#### Data availability statement

All data are original and were not published anywhere else.

#### References

- Aguilar-Islas, A. M., J. Wu, R. Rember, A. M. Johansen, and L. M. Shank. 2010. Dissolution of aerosol-derived iron in seawater: Leach solution chemistry, aerosol type, and colloidal iron fraction. *Mar. Chem.* **120**: 25–33. doi:10.1016/j.marchem.2009.01.011
- Alori, E. T., B. R. Glick, and O. O. Babalola. 2017. Microbial phosphorus solubilization and its potential for use in sustainable agriculture. *Front. Microbiol.* **8**: 1–8. doi:10.3389/fmicb.2017.00971
- Anderson, L. D., K. L. Faul, and A. Paytan. 2010. Phosphorus associations in aerosols: What can they tell us about P bioavailability? *Mar. Chem.* **120**: 44–56. doi:10.1016/j.marchem.2009.04.008
- Aydin, I., F. Aydin, A. Saydut, and C. Hamamci. 2009. A sequential extraction to determine the distribution of phosphorus in the seawater and marine surface sediment. *J. Hazard. Mater.* **168**: 664–669. doi:10.1016/j.jhazmat.2009.02.095
- Azam, F., and F. Malfatti. 2007. Microbial structuring of marine ecosystems. *Nat. Rev. Microbiol.* **5**: 782–791. doi:10.1038/nrmicro1747
- Baker, A. R., T. D. Jickells, M. Witt, and K. L. Linge. 2006. Trends in the solubility of iron, aluminium, manganese and phosphorus in aerosol collected over the Atlantic Ocean. *Mar. Chem.* **98**: 43–58. doi:10.1016/j.marchem.2005.06.004
- Baker, A. R., and others. 2021. Changing atmospheric acidity as a modulator of nutrient deposition and ocean biogeochemistry. *Sci. Adv.* **7**: 1–10. doi:10.1126/sciadv.abd8800
- Basu, S., and Y. Shaked. 2018. Mineral iron utilization by natural and cultured *Trichodesmium* and associated bacteria. *Limnol. Oceanogr.* **63**: 2307–2320. doi:10.1002/lno.10939
- Basu, S., M. Gledhill, D. de Beer, S. G. Matondkar, and Y. Shaked. 2019. Colonies of marine cyanobacteria *Trichodesmium* interact with associated bacteria to acquire iron from dust. *Commun. Biol.* **2**: 1–8. doi:10.1038/s42003-019-0534-z
- Bielski, B. H. J., D. E. Cabelli, R. L. Arudi, and A. B. Ross. 1985. Reactivity of HO<sub>2</sub>/O<sub>2</sub><sup>-</sup> radicals in aqueous solution. *J. Phys. Chem. Ref. Data Monogr.* **14**: 1041–1100. doi:10.1063/1.555739
- Borch, T., Y. Masue, R. K. Kukkadapu, and S. Fendorf. 2007. Phosphate imposed limitations on biological reduction and alteration of ferrihydrite. *Environ. Sci. Technol.* **41**: 166–172. doi:10.1021/es060695p
- Boyd, P. W., D. S. Mackie, and K. A. Hunter. 2010. Aerosol iron deposition to the surface ocean—Modes of iron supply and biological responses. *Mar. Chem.* **120**: 128–143. doi:10.1016/j.marchem.2009.01.008
- Browning, T. J., and others. 2022. Nutrient co-limitation in the subtropical Northwest Pacific. *Limnol. Oceanogr. Lett.* **7**: 52–61. doi:10.1002/lol2.10205
- Cerdan-Garcia, E., and others. 2022. Transcriptional responses of *Trichodesmium* to natural inverse gradients of Fe and P availability. *ISME J.* **16**: 1055–1064. doi:10.1038/s41396-021-01151-1
- Cui, K., and others. 2022. Siderophores, a potential phosphate solubilizer from the endophyte *Streptomyces* sp. CoT10, improved phosphorus mobilization for host plant growth and rhizosphere modulation. *J. Clean. Prod.* **367**: 133110. doi:10.1016/j.jclepro.2022.133110
- Dam, T. T. N., and others. 2021. X-ray spectroscopic quantification of phosphorus transformation in Saharan Dust during Trans-Atlantic Dust transport. *Environ. Sci. Technol.* **55**: 12694–12703. doi:10.1021/acs.est.1c01573
- Dansie, A. P., D. S. G. Thomas, G. F. S. Wiggs, M. C. Baddock, and I. Ashpole. 2022. Plumes and blooms—Locally-sourced Fe-rich aeolian mineral dust drives phytoplankton growth

- off southwest Africa. *Sci. Total Environ.* **829**: 154562. doi:[10.1016/j.scitotenv.2022.154562](https://doi.org/10.1016/j.scitotenv.2022.154562)
- Decho, A. W., and T. Gutierrez. 2017. Microbial extracellular polymeric substances (EPSs) in ocean systems. *Front. Microbiol.* **8**: 1–28. doi:[10.3389/fmicb.2017.00922](https://doi.org/10.3389/fmicb.2017.00922)
- de Leeuw, G., and others. 2014. Ocean–atmosphere interactions of particles, p. 171–246. *In* P. S. Liss and M. T. Johnson [eds.], *Ocean–atmosphere interactions of gases and particles*. Springer Earth System Sciences.
- Diaz, J. M., C. M. Hansel, B. M. Voelker, C. M. Mendes, P. F. Andeer, and T. Zhang. 2013. Widespread production of extracellular superoxide by heterotrophic bacteria. *Science* **340**: 1223–1227. doi:[10.1126/science.1237331](https://doi.org/10.1126/science.1237331)
- Duhamel, S., J. M. Diaz, J. C. Adams, K. Djaoudi, V. Steck, and E. M. Waggoner. 2021. Phosphorus as an integral component of global marine biogeochemistry. *Nat. Geosci.* **14**: 359–368. doi:[10.1038/s41561-021-00755-8](https://doi.org/10.1038/s41561-021-00755-8)
- Dyrhman, S. T. 2016. Nutrients and their acquisition: Phosphorus physiology in microalgae, p. 155–183. *In* M. Borowitzka, J. Beardall, and J. Raven [eds.], *The physiology of microalgae, developments in applied phycology*, v. **6**. Springer.
- Dyrhman, S. T., P. D. Chappell, S. T. Haley, J. W. Moffett, E. D. Orchard, J. B. Waterbury, and E. A. Webb. 2006. Phosphonate utilization by the globally important marine diazotroph *Trichodesmium*. *Nature* **439**: 68–71. doi:[10.1038/nature04203](https://doi.org/10.1038/nature04203)
- Egger, M., T. Jilbert, T. Behrends, C. Rivard, and C. P. Slomp. 2015. Vivianite is a major sink for phosphorus in methanogenic coastal surface sediments. *Geochim. Cosmochim. Acta* **169**: 217–235. doi:[10.1016/j.gca.2015.09.012](https://doi.org/10.1016/j.gca.2015.09.012)
- Eichner, M., S. Basu, S. Wang, D. de Beer, and Y. Shaked. 2020. Mineral iron dissolution in *Trichodesmium* colonies: The role of O<sub>2</sub> and pH microenvironments. *Limnol. Oceanogr.* **65**: 1149–1160. doi:[10.1002/lno.11377](https://doi.org/10.1002/lno.11377)
- Ellwood, M. J., and others. 2018. Insights into the biogeochemical cycling of iron, nitrate, and phosphate across a 5,300 km South Pacific Zonal Section (153°E–150°W). *Global Biogeochem. Cycl.* **32**: 187–207. doi:[10.1002/2017GB005736](https://doi.org/10.1002/2017GB005736)
- Elser, J. J., and others. 2007. Global analysis of nitrogen and phosphorus limitation of primary producers in freshwater, marine and terrestrial ecosystems. *Ecol. Lett.* **10**: 1135–1142. doi:[10.1111/j.1461-0248.2007.01113.x](https://doi.org/10.1111/j.1461-0248.2007.01113.x)
- Fitzsimmons, J. N., S. G. John, C. M. Marsay, C. L. Hoffman, S. L. Nicholas, B. M. Toner, C. R. German, and R. M. Sherrell. 2017. Iron persistence in a distal hydrothermal plume supported by dissolved-particulate exchange. *Nat. Geosci.* **10**: 195–201. doi:[10.1038/ngeo2900](https://doi.org/10.1038/ngeo2900)
- Frischkorn, K. R., M. Rouco, B. A. S. Van Mooy, and S. T. Dyrhman. 2017. Epibionts dominate metabolic functional potential of *Trichodesmium* colonies from the oligotrophic ocean. *ISME J.* **11**: 2090–2101. doi:[10.1038/ismej.2017.74](https://doi.org/10.1038/ismej.2017.74)
- Gledhill, M., S. Basu, and Y. Shaked. 2019. Metallophores associated with: *Trichodesmium erythraeum* colonies from the Gulf of Aqaba. *Metallomics* **11**: 1547–1557. doi:[10.1039/c9mt00121b](https://doi.org/10.1039/c9mt00121b)
- Grossart, H. P., T. Kiørboe, K. Tang, and H. Ploug. 2003. Bacterial colonization of particles: Growth and interactions. *Appl. Environ. Microbiol.* **69**: 3500–3509. doi:[10.1128/AEM.69.6.3500-3509.2003](https://doi.org/10.1128/AEM.69.6.3500-3509.2003)
- Gunnars, A., S. Blomqvist, P. Johansson, and C. Andersson. 2002. Formation of Fe(III) oxyhydroxide colloids in freshwater and brackish seawater, with incorporation of phosphate and calcium. *Geochim. Cosmochim. Acta* **66**: 745–758. doi:[10.1016/S0016-7037\(01\)00818-3](https://doi.org/10.1016/S0016-7037(01)00818-3)
- Hansel, C. M., C. Buchwald, J. M. Diaz, J. E. Ossolinski, S. T. Dyrhman, B. A. S. Van Mooy, and D. Polyviou. 2016. Dynamics of extracellular superoxide production by *Trichodesmium* colonies from the Sargasso Sea. *Limnol. Oceanogr.* **61**: 1188–1200. doi:[10.1002/lno.10266](https://doi.org/10.1002/lno.10266)
- Held, N. A., and others. 2020. Co-occurrence of Fe and P stress in natural populations of the marine diazotroph *Trichodesmium*. *Biogeosciences* **17**: 2537–2551. doi:[10.5194/bg-17-2537-2020](https://doi.org/10.5194/bg-17-2537-2020)
- Held, N. A., and others. 2021. Mechanisms and heterogeneity of in situ mineral processing by the marine nitrogen fixer *Trichodesmium* revealed by single-colony metaproteomics. *ISME Commun.* **1**: 1–9. doi:[10.1038/s43705-021-00034-y](https://doi.org/10.1038/s43705-021-00034-y)
- Hettiarachchi, E., S. Ivanov, T. Kieft, H. L. Goldstein, B. M. Moskowitz, R. L. Reynolds, and G. Rubasinghege. 2021. Atmospheric processing of iron-bearing mineral dust aerosol and its effect on growth of a marine diatom, *Cyclotella meneghiniana*. *Environ. Sci. Technol.* **55**: 871–881. doi:[10.1021/acs.est.0c06995](https://doi.org/10.1021/acs.est.0c06995)
- Hudson, R. J. M., and F. M. M. Morel. 1989. Distinguishing between extra- and intracellular iron in marine phytoplankton. *Limnol. Oceanogr.* **34**: 1113–1120. doi:[10.4319/lo.1989.34.6.1113](https://doi.org/10.4319/lo.1989.34.6.1113)
- Jaisi, D. P., R. E. Blake, and R. K. Kukkadapu. 2010. Fractionation of oxygen isotopes in phosphate during its interactions with iron oxides. *Geochim. Cosmochim. Acta* **74**: 1309–1319. doi:[10.1016/j.gca.2009.11.010](https://doi.org/10.1016/j.gca.2009.11.010)
- Journet, E., K. V. Desboeufs, S. Caquineau, and J. L. Colin. 2008. Mineralogy as a critical factor of dust iron solubility. *Geophys. Res. Lett.* **35**: 3–7. doi:[10.1029/2007GL031589](https://doi.org/10.1029/2007GL031589)
- Kappler, A., C. Bryce, M. Mansor, U. Lueder, J. M. Byrne, and E. D. Swanner. 2021. An evolving view on biogeochemical cycling of iron. *Nat. Rev. Microbiol.* **19**: 360–374. doi:[10.1038/s41579-020-00502-7](https://doi.org/10.1038/s41579-020-00502-7)
- Kessler, N., R. Armoza-Zvuloni, S. Wang, S. Basu, P. K. Weber, R. K. Stuart, and Y. Shaked. 2020a. Selective collection of iron-rich dust particles by natural *Trichodesmium* colonies. *ISME J.* **14**: 91–103. doi:[10.1038/s41396-019-0505-x](https://doi.org/10.1038/s41396-019-0505-x)
- Kessler, N., S. M. Kraemer, Y. Shaked, and W. D. C. Schenkeveld. 2020b. Investigation of siderophore-promoted and reductive dissolution of dust in marine

- microenvironments such as *Trichodesmium* colonies. *Front. Mar. Sci.* **7**: 1–15. doi:10.3389/fmars.2020.00045
- Koedooder, C., E. Landou, F. Zhang, S. Wang, S. Basu, I. Berman-Frank, Y. Shaked, and M. Rubin-Blum. 2022. Metagenomes of Red Sea subpopulations challenge the use of marker genes and morphology to assess *Trichodesmium* diversity. *Front. Microbiol.* **13**. doi:10.3389/fmicb.2022.879970
- Kraal, P., C. M. Van Genuchten, W. K. Lenstra, and T. Behrends. 2020. Coprecipitation of phosphate and silicate affects environmental iron (oxyhydr)oxide transformations: A gel-based diffusive sampler approach. *Environ. Sci. Technol.* **54**: 12795–12802. doi:10.1021/acs.est.0c02352
- Kranzler, C., N. Kessler, N. Keren, and Y. Shaked. 2016. Enhanced ferrihydrite dissolution by a unicellular, planktonic cyanobacterium: A biological contribution to particulate iron bioavailability. *Environ. Microbiol.* **18**: 5101–5111. doi:10.1111/1462-2920.13496
- Lam, P. J., and J. K. B. Bishop. 2008. The continental margin is a key source of iron to the HNLC North Pacific Ocean. *Geophys. Res. Lett.* **35**: 1–5. doi:10.1029/2008GL033294
- Langlois, R. J., M. M. Mills, C. Ridame, P. Croot, and J. LaRoche. 2012. Diazotrophic bacteria respond to Saharan dust additions. *Mar. Ecol. Prog. Ser.* **470**: 1–14. doi:10.3354/meps10109
- Li, M., J. Liu, Y. Xu, and G. Qian. 2016. Phosphate adsorption on metal oxides and metal hydroxides: A comparative review. *Environ. Rev.* **24**: 319–332. doi:10.1139/er-2015-0080
- Mahowald, N. M., D. S. Hamilton, K. R. M. Mackey, J. K. Moore, A. R. Baker, R. A. Scanza, and Y. Zhang. 2018. Aerosol trace metal leaching and impacts on marine microorganisms. *Nat. Commun.* **9**: 2614. doi:10.1038/s41467-018-04970-7
- Marcotte, A. R., A. D. Anbar, B. J. Majestic, and P. Herckes. 2020. Mineral dust and iron solubility: Effects of composition, particle size, and surface area. *Atmosphere* **11**: 533–545. doi:10.3390/atmos11050533
- McConnell, C. A., J. P. Kaye, and A. R. Kemanian. 2020. Reviews and syntheses: Ironing out wrinkles in the soil phosphorus cycling paradigm. *Biogeosciences* **17**: 5309–5333. doi:10.5194/bg-17-5309-2020
- McRose, D. L., and D. K. Newman. 2021. Redox-active antibiotics enhance phosphorus bioavailability. *Science* **371**: 1033–1037. doi:10.1126/science.abd1515
- Melton, E. D., E. D. Swanner, S. Behrens, C. Schmidt, and A. Kappler. 2014. The interplay of microbially mediated and abiotic reactions in the biogeochemical Fe cycle. *Nat. Rev. Microbiol.* **12**: 797–808. doi:10.1038/nrmicro3347
- Moore, C. M., and others. 2013. Processes and patterns of oceanic nutrient limitation. *Nat. Geosci.* **6**: 701–710. doi:10.1038/ngeo1765
- Morris, J. J., A. L. Rose, and Z. Lu. 2022. Reactive oxygen species in the world ocean and their impacts on marine ecosystems. *Redox Biol.* **52**: 102285. doi:10.1016/j.redox.2022.102285
- Mulholland, M. R., S. Floge, E. J. Carpenter, and D. G. Capone. 2002. Phosphorus dynamics in cultures and natural populations of *Trichodesmium* spp. *Mar. Ecol. Prog. Ser.* **239**: 45–55. doi:10.3354/meps239045
- Nenes, A., M. D. Krom, N. Mihalopoulos, P. Van Cappellen, Z. Shi, A. Bougiatioti, P. Zampas, and B. Herut. 2011. Atmospheric acidification of mineral aerosols: A source of bioavailable phosphorus for the oceans. *Atmos. Chem. Phys.* **11**: 6265–6272. doi:10.5194/acp-11-6265-2011
- Paytan, A., and K. McLaughlin. 2007. The oceanic phosphorus cycle. *Chem. Rev.* **107**: 563–576. doi:10.1021/cr0503613
- Perron, M. M. G., M. Strzelec, M. Gault-Ringold, B. C. Proemse, P. W. Boyd, and A. R. Bowie. 2020. Assessment of leaching protocols to determine the solubility of trace metals in aerosols. *Talanta* **208**: 120377. doi:10.1016/j.talanta.2019.120377
- Qiu, G. W., C. Koedooder, B. S. Qiu, Y. Shaked, and N. Keren. 2022. Iron transport in cyanobacteria—From molecules to communities. *Trends Microbiol.* **30**: 229–240. doi:10.1016/j.tim.2021.06.001
- Romano, S., V. Bondarev, M. Kölling, T. Dittmar, and H. N. Schulz-Vogt. 2017. Phosphate limitation triggers the dissolution of precipitated iron by the marine bacterium *Pseudovibrio* sp. FO-BEG1. *Front. Microbiol.* **8**: 1–11. doi:10.3389/fmicb.2017.00364
- Rose, A. L., T. P. Salmon, T. Lukondeh, B. A. Neilan, and T. D. Waite. 2005. Use of superoxide as an electron shuttle for iron acquisition by the marine cyanobacterium *Lyngbya majuscula*. *Environ. Sci. Technol.* **39**: 3708–3715. doi:10.1021/es048766c
- Rubin, M., I. Berman-Frank, and Y. Shaked. 2011. Dust- and mineral-iron utilization by the marine dinitrogen-fixer *Trichodesmium*. *Nat. Geosci.* **4**: 529–534. doi:10.1038/ngeo1181
- Rueter, J. G., D. A. Hutchins, R. W. Smith, and N. L. Unsworth. 1992. Iron nutrition in *Trichodesmium*, p. 289–306. In E. J. Carpenter, D. G. Capone, and J. G. Rueter [eds.], *Marine pelagic cyanobacteria: Trichodesmium and other diazotrophs*. Kluwer Academic.
- Ruttenberg, K. C., and D. J. Sulak. 2011. Sorption and desorption of dissolved organic phosphorus onto iron (oxyhydr) oxides in seawater. *Geochim. Cosmochim. Acta* **75**: 4095–4112. doi:10.1016/j.gca.2010.10.033
- Schwertmann, U., and R. M. Cornell. 2008. Iron oxides in the laboratory: Preparation and characterization. John Wiley & Sons.
- Seymour, J. R., S. A. Amin, J. B. Raina, and R. Stocker. 2017. Zooming in on the phycosphere: The ecological interface for phytoplankton–bacteria relationships. *Nat. Microbiol.* **2**: 17065. doi:10.1038/nmicrobiol.2017.65
- Shaked, Y., A. B. Kustka, and F. M. M. Morel. 2005. A general kinetic model for iron acquisition by eukaryotic

- phytoplankton. *Limnol. Oceanogr.* **50**: 872–882. doi:10.4319/lo.2005.50.3.0872
- Shi, J., N. Wang, H. Gao, A. R. Baker, X. Yao, and D. Zhang. 2019. Phosphorus solubility in aerosol particles related to particle sources and atmospheric acidification in Asian continental outflow. *Atmos. Chem. Phys.* **19**: 847–860. doi:10.5194/acp-19-847-2019
- Simon, M., H. P. Grossart, B. Schweitzer, and H. Ploug. 2002. Microbial ecology of organic aggregates in aquatic ecosystems. *Aquat. Microb. Ecol.* **28**: 175–211. doi:10.3354/ame028175
- Stihl, A., U. Sommer, and A. F. Post. 2001. Alkaline phosphatase activities among populations of the colony-forming diazotrophic cyanobacterium *Trichodesmium* spp. (cyanobacteria) in the red sea. *J. Phycol.* **37**: 310–317. doi:10.1046/j.1529-8817.2001.037002310.x
- Swanner, E. D., and others. 2015. Physiology, Fe(II) oxidation, and Fe mineral formation by a marine planktonic cyanobacterium grown under ferruginous conditions. *Front. Earth Sci.* **3**: 1–21. doi:10.3389/feart.2015.00060
- Swanner, E. D., M. Maisch, W. Wu, and A. Kappler. 2018. Oxidative Fe(III) reduction could have generated Fe(II) in the photic zone of Precambrian seawater. *Sci. Rep.* **8**: 1–9. doi:10.1038/s41598-018-22694-y
- Tagliabue, A., A. R. Bowie, P. W. Boyd, K. N. Buck, K. S. Johnson, and M. A. Saito. 2017. The integral role of iron in ocean biogeochemistry. *Nature* **543**: 51–59. doi:10.1038/nature21058
- Tang, D., and F. M. M. Morel. 2006. Distinguishing between cellular and Fe-oxide-associated trace elements in phytoplankton. *Mar. Chem.* **98**: 18–30. doi:10.1016/j.marchem.2005.06.003
- Tipping, E., and others. 2014. Atmospheric deposition of phosphorus to land and freshwater. *Environ. Sci. Process. Impacts* **16**: 1608–1617. doi:10.1039/c3em00641g
- Uroz, S., L. Picard, and M. P. Turpault. 2022. Recent progress in understanding the ecology and molecular genetics of soil mineral weathering bacteria. *Trends Microbiol.* **30**: 882–897. doi:10.1016/j.tim.2022.01.019
- Walworth, N. G., F. X. Fu, E. A. Webb, M. A. Saito, D. Moran, M. R. McIlvin, M. D. Lee, and D. A. Hutchins. 2016. Mechanisms of increased *Trichodesmium* fitness under iron and phosphorus co-limitation in the present and future ocean. *Nat. Commun.* **7**: 1–11. doi:10.1038/ncomms12081
- Wang, S., C. Koedooder, F. Zhang, N. Kessler, M. Eichner, D. Shi, and Y. Shaked. 2022. Colonies of the marine cyanobacterium *Trichodesmium* optimize dust utilization by selective collection and retention of nutrient-rich particles. *iScience* **25**: 103587. doi:10.1016/j.isci.2021.103587
- Weinberger, R., T. Weiner, and A. Angert. 2016. Isotopic signature of atmospheric phosphate emitted from coal combustion. *Atmos. Environ.* **136**: 22–30. doi:10.1016/j.atmosenv.2016.04.006

#### Acknowledgments

The authors thank Coco Koedooder and Murielle Dray for valuable assistance along the study and manuscript writing. Our research was supported by the Israel Science Foundation grant 260/21 ([www.isf.org.il](http://www.isf.org.il)) awarded to Y.S., the PBC Postdoctoral fellowship awarded to S.B. and F.Z. and the CSC-HUJI doctoral fellowship awarded to S.W.

#### Conflict of Interest

The authors declare no conflict of interests.

Submitted 28 August 2022

Revised 11 December 2022

Accepted 12 February 2023

Associate editor: Hans-Peter Grossart